European Polymer Journal 252 (2026) 114747

Contents lists available at ScienceDirect

European Polymer Journal

journal homepage: www.elsevier.com/locate/europolj

# Biodegradable Poly(dodecane succinate-ran-caprolactone) nanoparticles with isodimorphic behavior for sustained release of CPT-11 in triple negative breast cancer

Roberta Cillari [a], Juan Torres-Rodríguez [b], Sergio Scirè [a], Ricardo Pérez-Camargo [b], Giuseppina Roscigno [c], Alejandro J. Müller [b,d,*], Nicolò Mauro [a,*]

[a] Laboratory of Pharmaceutical Advanced Nanotechnologies & Translational Research – PANTRLab, Department of "Scienze e Tecnologie Biologiche, Chimiche e Farmaceutiche" (STEBICEF), University of Palermo, Via Archirafi 32, 90123 Palermo, Italy
[b] POLYMAT and Department of Polymers and Advanced Materials: Physics, Chemistry and Technology, Faculty of Chemistry, University of the Basque Country UPV/EHU, Paseo Manuel de Lardizabal, 3, 20018 Donostia-San Sebastián, Spain
[c] Department of Biology, "Federico II" University of Naples, Via Cinthia 21, 80126 Napoli, Italy
[d] IKERBASQUE, Basque Foundation for Science, Plaza Euskadi 5, 48009 Bilbao, Spain

ARTICLE INFO

*Keywords:*
Poly(dodecane succinate-ran-caprolactone)
Irinotecan
Breast cancer
Nanoparticles
Drug delivery

ABSTRACT

Engineering semicrystalline microstructures in biodegradable polymers offers a powerful yet underexplored strategy to regulate drug–matrix interactions and pharmaceutical performance. Here, we report isodimorphic poly(dodecane succinate-*ran*-caprolactone) (DS–CL) random copolymers as structurally tunable platforms for nanoparticle-mediated delivery of CPT-11 in triple-negative breast cancer (TNBC). Differential scanning calorimetry and synchrotron wide-angle X-ray scattering revealed composition-dependent pseudoeutectic behavior, demonstrating that subtle variations in comonomer content modulate thermal properties, crystallinity, and unit-cell parameters. These structural differences directly governed nanoparticle formation, drug affinity, and colloidal stability. All copolymers yielded spherical nanoparticles (~100–150 nm) via a sustainable acetone-based nanoprecipitation method. However, only the low-crystallinity, PCL-rich composition ($DS_{11}CL_{89}$) enabled stable CPT-11 encapsulation, underscoring the decisive role of the PCL-type crystalline phase in drug–polymer interactions. Drug-loaded nanoparticles exhibited sustained release (~50% at 24 h) with pH-dependent kinetics and enhanced surface charge stability. Whereas unloaded nanoparticles were cytocompatible in normal breast epithelial cells, with negligible toxic effects in cancer cells, CPT-11-loaded formulations induced dose-dependent cytotoxicity selectively in MDA-MB-231 TNBC cells with reduced acute toxicity compared to free drug, consistent with controlled intracellular release. This study establishes a direct structure–property–function relationship in isodimorphic random copolyesters, positioning crystalline microstructure engineering as a rational design principle for precision nanomedicine targeting aggressive breast cancer subtypes.

## 1. Introduction

Polymeric materials, due to their combination of biocompatibility and tunable physicochemical properties, have gained meaningful interest in the field of biomedical applications [1–4]. Polyesters stand out for their unique features, including biocompatibility and degradability, as well as synthetic versatility, despite some limitations in terms of their thermal and mechanical properties [3,5]. Poly(lactic acid) (PLA), poly (ε-caprolactone) (PCL), and poly(lactic-co-glycolic acid) (PLGA), or related copolymers, are among the most widely employed biodegradable polymers for drug delivery applications[6]. Despite their widespread use, PLA- and PLGA-based systems offer limited tunability of their physicochemical properties, which restricts their application as drug carriers to compounds with suitable hydrophobicity. On the other hand, the excessively slow degradation rate of PCL-based systems can hinder precise control over drug release profiles.

Therefore, designing novel copolymers could help overcome these issues and lead to the development of materials that can be exploited in

* Corresponding authors.
*E-mail addresses:* alejandrojesus.muller@ehu.es (A.J. Müller), nicolo.mauro@unipa.it (N. Mauro).

https://doi.org/10.1016/j.eurpolymj.2026.114747
Received 13 March 2026; Received in revised form 14 April 2026; Accepted 15 April 2026
Available online 16 April 2026

various medical applications. Copolymerization is used to tailor the physicochemical properties of polymers such as PCL. PCL has been widely used in FDA-approved medical devices and it is also known for its superb biodegradability, cost-effectiveness, and biocompatibility[7]. The combination of PCL with other polymers, either through random or block copolymerization, has been extensively investigated to develop novel materials exhibiting enhanced performance and improved physicochemical properties. [8,9] Among the various strategies available, random copolymerization represents a practical approach to avoid the phase separation issues commonly encountered in block copolymers or blends. When both components of the random copolymers are potentially semicrystalline, as in the materials used in this work, many complex phenomena may arise due to the chemical structures and compositions of their co-monomeric units. Among them, a particularly remarkable one is isodimorphic behavior, which has been extensively studied due to its tunable properties arising from a comonomer inclusion/exclusion mechanism. [10–15] This controllable crystallization behavior enables precise modulation of polymer morphology and degradation kinetics, offering significant potential for optimizing drug release profiles in advanced delivery systems. An interesting isodimorphic random PCL-based copolymeric system is the high-molecular-weight poly(dodecane succinate-*ran*-caprolactone) (DS-CL), which has been synthesized with varying compositions and exhibits the three main characteristics that identify isodimorphic behavior, as reported in the literature. [16–19] These characteristics are: (i) crystallization across the entire composition range; (ii) a pseudo eutectic trend in the melting temperature when plotted as a function of copolymer composition, characterized by a V-shaped, with a transition point between the two types of different crystalline phases formed, and (iii) a variation in the crystalline unit cell parameters at both sides of the pseudoeutectic point, reflecting comonomer inclusion. The observed variations in thermal and structural properties[20] make these copolymers promising candidates for biomedical applications, such as drug delivery. In fact, the unique tunability in crystallinity is expected to directly affect polymer chain packing, amorphous/crystalline balance, and chain mobility, which in turn may influence nanoparticle formation, drug accommodation within the matrix, and release kinetics.

Polymeric nanoparticles based on polyesters have garnered significant attention in drug delivery, as they possess tailorable chemical properties, high biocompatibility, and remarkable biocompatibility and biodegradability[21]. The properties of nanoparticles, such as charge, surface chemistry, and size, can be modulated by optimizing the synthesis protocol to ensure prolonged circulation and preferential extravasation at the tumor site via the enhanced permeability and retention (EPR) effect[22]. Besides, undergoing pH-dependent and enzyme-mediated degradation in biological environments, polyester-nanoparticles provide unique opportunities for developing stimulus-responsive carriers, ensuring prolonged release of the drug payload at the target site [23]. However, the main weakness of nanoparticles remains the low drug loading capability (1–6%), which limits their use to the delivery of potent drugs. Here, DS-CL copolymers with different compositions were used to obtain DS-CL nanoparticles with the desired characteristics. Irinotecan hydrochloride (CPT-11), an antineoplastic chemotherapy drug belonging to the camptothecin class, was used as a model drug to evaluate the suitability of the developed nanoparticles as nanocarriers and to explore their potential application in cancer treatment. [24].

## 2. Materials and methods

Dimethyl succinate (DMS) (99.5%), 1,12-dodecanediol (DD) (99.5%), ε-caprolactone (CL), titanium tetraisopropoxide (TTP) (>99%), methanol (MeOH) (>99.5%), chloroform ($CHCl_3$) (99.8%), Poly(ethylene glycol) 4 kDa (PEG), poly(ethylene glycol) 10 kDa (PEG), polyvinylpirrolidone 30 kDa (PVP), acetone (>99.5%), CPT-11 (>97%), SpectraPor® Pre-wetted RC Tubing (MWCO 1 kDa), Dulbecco's Modified Eagle's Medium (DMEM), fetal bovine serum (FBS), L-glutamine (99%), penicillin (98.5%), streptomycin (98.5%), and amphotericin B (98%) were purchased from Sigma-Aldrich and utilized as supplied without further purification. The CellTiter 96 AQueous One Solution Cell Proliferation Assay (MTS) was purchased from Promega (Milan, Italy).

Human breast cancer cell line MDA-MB-231 and MCF-10A were obtained from "Istituto Zooprofilattico Sperimentale della Lombardia e dell'Emilia Romagna", Italy.

### 2.1. Copolymers synthesis

The high molecular weight dodecane succinate-*ran*-caprolactone (DS-CL) copolymers of different compositions were synthesized through a two-step procedure. In the first step, ε-caprolactone (CL, 2 mmol), dimethyl succinate (DS, 1.1 mmol), and 1,12-dodecanediol (DD, 1 mmol) were mixed at 160 °C under mechanical stirring (60 rpm) for 24 h. Titanium isopropoxide (TTP, 400 ppm) was used as the catalyst for the reaction. In the second step, the temperature was increased to 220 °C under high vacuum ($10^{-6}$ mbar) for 24 h. The same synthetic procedure (Scheme. S1) was used to obtain copolymers with varying compositions, as summarized in Table 1. Copolymer compositions were determined by $^1$H NMR using characteristic signals of the PDS and PCL units, as shown in Fig. S1.

The parent homopolymers (PCL and PDS) were also synthesized for comparison purposes. For PDS synthesis, the same two-step synthesis procedure used for the copolymers was used. In contrast, the synthesis of PCL required only a single step. ε-Caprolactone was polymerized using the same catalyst concentration (400 ppm) at 120 °C, with continuous stirring at 60 rpm for 6 h. Finally, a purification in methanol was performed, obtaining a white solid which is stored in a freezer (−4 °C).

### 2.2. Copolymers characterization

#### 2.2.1. 1.3.1 Differential scanning calorimetry (DSC)

DSC experiments were conducted using a PerkinElmer 8500 calorimeter equipped with an Intracooler 3 refrigerated cooling system, operating under an ultra-pure nitrogen atmosphere at a flow rate of 20 mL $min^{-1}$. The instrument was calibrated using high-purity standards of indium and tin. Samples, weighing approximately 3 mg, were hermetically sealed in standard aluminum pans and subjected to the following non-isothermal thermal protocol: Samples were heated from room temperature to a given temperature ($T$) 30 °C above their melting temperature ($T_m$) (first heating) and held at $T$ for 3 min to erase their thermal history. Subsequently, they were cooled to −40 °C at 20 °C $min^{-1}$, held at this temperature for 1 min, and then reheated (second heating) to $T$ at 20 °C $min^{-1}$ to create a standard thermal history.

The degree of crystallinity was determined from the DSC first heating scans after film formation according to:

$$X_c = \frac{\Delta H_m}{\Delta H_m^0 f} \times 100$$

**Table 1**
Characteristics of the DS-CL copolymers obtained by the synthetic procedure.

| Sample | Composition (% mol)[a] | | Molecular weight[b] | | |
|---|---|---|---|---|---|
| | DS | CL | $\overline{M}_n$(g/mol) | $\overline{M}_w$(g/mol) | $Đ$ |
| PDS | 100 | 0 | 48,700 | 163,300 | 3.4 |
| $DS_{71}CL_{29}$ | 71 | 29 | 94,000 | 253,000 | 2.7 |
| $DS_{44}CL_{56}$ | 44 | 56 | 87,600 | 201,400 | 2.3 |
| $DS_{11}CL_{89}$ | 11 | 89 | 83,200 | 161,500 | 1.9 |
| PCL | 0 | 100 | 54,200 | 93,100 | 1.7 |

[a] Composition of the polymer as determined by $^1$H NMR.
[b] Number and weight average molecular weights and dispersities estimated by GPC.

where $\Delta H_m$ is the measured melting enthalpy, $\Delta H_m^0$ is the enthalpy of fusion for a 100% crystalline sample (Polycaprolactone = 139.5 J $g^{-1}$ [25] and Poly(dodecane succinate) = 200.1 J $g^{-1}$ [20]) and $f$ is the weight fraction of the crystallizable monomer in the copolymer.

#### 2.2.2. Dynamic mechanical thermal analysis (DMTA)

A Dynamic Mechanical Thermal Analyzer, the Triton 2000 DMA from Triton Technology, was used in bending deformation mode (single cantilever measuring system) for rectangular specimens (length, width, and thickness of 30 x 6 x 2 mm, respectively) cut from the compression-molded sheets. The tests were performed at 1 Hz and a heating rate of 4 °C $min^{-1}$ from −100 °C to 20 °C. Measurements were carried out to determine the glass transition temperature ($T_g$), taken as the maximum peak in the loss tangent, tan $\delta$.

#### 2.2.3. Wide-angle X-ray scattering (WAXS)

In situ WAXS analysis was performed at beamline BL11-NCD at the ALBA synchrotron radiation facility in Barcelona, Spain. Samples enclosed in DSC pans were positioned on a Linkam THMS600 stage connected to a liquid nitrogen cooling system, and the same non-isothermal measurement employed in DSC was performed. Throughout this procedure, WAXS spectra were recorded every 1 s.

WAXS scans were performed periodically at two scans per °C. The X-ray source operated at an energy of 12.4 keV (λ = 1.0 Å). In the WAXS configuration, the sample–detector distance (WAXS detector, Rayonix LX255-HS with an active area of 230.4 × 76.8 mm and a pixel size of 44 × 44 $\mu m^2$) was 15.5 mm, with a tilt angle of 27.3°. The scattering vector, $q = 4\pi \sin \theta \lambda^{-1}$, where $\lambda$ represents the X-ray wavelength ($\lambda$ = 1 Å) and $2\theta$ denotes the scattering angle. The intensity profile was presented as the scattering intensity plotted against the scattering angle ($2\theta$). Calibration of the scattering vector was conducted using chromium (III) oxide.

### 2.3. Preparation of DS-CL nanoparticles

Initially, 5 mg of each copolymer were dissolved in 1 mL of acetone (5 mg $mL^{-1}$), and then acetone was added up to 10 mL. To induce nanoprecipitation, 2 mL of distilled water were rapidly added to the acetone solution under continuous magnetic stirring. The organic solvent was removed by rotary evaporation, and during this step, 3 mL of water were gradually poured into the solution. Subsequently, the nanoparticles' dispersions (NPs $DS_{44}CL_{56}$, NPs $DS_{71}CL_{29}$, and NPs $DS_{11}CL_{89}$) were aliquoted to test the efficacy of two different types of cryoprotectant agents (PEG 4 kDa 5% w/v, PEG 10 kDa 5% w $v^{-1}$). Finally, the dispersions were rapidly frozen using liquid nitrogen and freeze-dried.

### 2.4. Characterization of DS-CL nanoparticles

For scanning electron microscopy (SEM) characterization, a FEI Tecnai G2 S-TWIN microscope operating at 200 kV and equipped with a 4 K camera (Thermo Fisher Scientific) was employed. To prepare the sample for observation, the freeze-dried powder of each sample was placed on a carbon tape, which was sputtered with 4 nm gold nanoparticles before analysis.

Dynamic light scattering (DLS) measurements were performed on 1 mL of nanoparticle dispersions (0.1 mg $mL^{-1}$), both before and after freeze-drying, with and without cryoprotectant, at 25 °C using a Malvern Zetasizer Nano ZS instrument (Rome, Italy) equipped with a 532 nm laser with a fixed scattering angle of 173°, and the Dispersion Technology Software 7.02 software (Malvern Panalytical ltd, Almelo, The Netherlands). Zeta-potential measurements were performed by aqueous electrophoresis, recorded at 25 °C using the same apparatus as for the DLS measurement. The Zeta-potential values (mV) were calculated from electrophoretic mobility using the Smoluchowski relationship. The nanoparticle dispersions were analyzed using a suitable amount of each sample to give an attenuator value of 7. All analyses were performed in triplicate, and results are expressed as mean values ± standard deviation (n = 3).

The colloidal stability of the nanoparticles in water over time (0, 3, 6, and 10 days) was evaluated by monitoring the Z-average size under the same conditions described above.

### 2.5. Incorporation of CPT-11 into $DS_{11}CL_{89}$ nanoparticles

Drug-loaded nanoparticles were successfully produced only using the $DS_{11}CL_{89}$ copolymer, as attempts with other copolymers did not result in stable formulations. 5 mg of the $DS_{11}CL_{89}$ copolymer and 1 mg (20% w/w) of irinotecan hydrochloride (CPT-11) were pounded in a mortar using acetone (added in four aliquots of 0.5 mL each) to wet the powders, forming a viscous paste during the solvent evaporation. After 30 min of manual grinding, the paste was diluted with acetone (10 mL), and the nanoprecipitation was performed by rapidly adding 3 mL of water under stirring. To remove the unloaded drug and acetone, the nanoparticle dispersion was dialyzed against ultrapure water using a 1 kDa molecular weight cut-off membrane.

### 2.6. Drug loading and release study of NPs $DS_{11}CL_{89}$@CPT-11

The nanoparticle $DS_{11}CL_{89}$@CPT-11 dispersion (1 mL) was filtered (5 μm CA), frozen, and freeze-dried. Then, the powder was reconstituted in the HPLC mobile phase. The resultant solution was then filtered through a 0.22 μm RC filter, and analyzed by HPLC. HPLC analysis was carried out by using an Agilent 1260 Infinity II instrument equipped with a Quaternary Pump VL G7111A and a VWD detector G7114A, 20 μl injector, and a computer integrating apparatus (OpenLAB CDS ChemStation Workstation). A reversed-phase column Luna Phenomenex C18 was used as the stationary phase at 25 °C, and a mixture of deionized water with 0.1% acetic acid/acetonitrile (70:30) was used as the mobile phase with a flow rate of 0.6 ml $min^{-1}$. The UV detector was fixed at 260 ± 4 nm. A calibration curve in the range of 1.5–75 μg $ml^{-1}$ (y = 84.103x, R = 0.999) was used to quantify CPT-11.

For drug release studies, a dispersion of $DS_{11}CL_{89}$@CPT-11 nanoparticles (5 mL), corresponding to a drug concentration of 0.22 mg $mL^{-1}$, was placed into a dialysis membrane (MWCO 2 kDa) against 15 mL of external medium (with 0.1%w/v Tween 80) at 37 °C under orbital stirring (100 rpm). The release experiments were conducted using either phosphate buffer (PBS, pH 7.4) or acetate buffer (pH 5.5). At defined time points, 0.5 mL of the external medium was withdrawn and replaced with an equal volume of fresh buffer, up to 24 h. The amount of CPT-11 released was quantified by HPLC analysis, using the method described above.

### 2.7. Cell culture conditions

TNBC cells (MDA-MB-231) were grown in Dulbecco's Minimum Essential Medium (DMEM), supplemented with 10% fetal bovine serum (FBS, Euroclone), 1% of penicillin/streptomycin (10000 U $mL^{-1}$ penicillin and 10 mg $mL^{-1}$ streptomycin, Euroclone) and 1% of L-glutamine (Euroclone), at 37 °C in 5% $CO_2$ humidified atmosphere. MCF-10A were cultured in DMEM/F-12 50:50 (Gibco™, Thermo Fisher Scientific), 1X B27 (Life Technologies, Milan Italy), 10 ng $mL^{-1}$ EGF (Sigma, Milan, Italy), 20 ng $mL^{-1}$ βFGF (Sigma, Milan, Italy), and 1X antibiotic–antimycotics (Life technologies, Milan, Italy).

Cells were kept in humidified incubator at 37 °C and 5% of $CO_2$.

### 2.8. Uptake studies of DS-CL nanoparticles

A preliminary evaluation of DS-CL nanoparticles' fluorescence emission was performed to establish the self-trackability of the prepared NPs in the DAPI ($\lambda_{EX}$ 340 nm) and FITC ($\lambda_{EX}$ 490 nm) channels. The cellular internalization of DS-CL NPs was evaluated by the MDA-MB-231 cell line by widefield fluorescence microscopy (Axio Cam MRm, Zeiss,

Oberkochen, Germany). Cells were seeded in an 8-well chambered coverglass (LabTek I) at a density of $5.0 \times 10^3$ cells per well (200 μL) and grown in DMEM. After 24 h, cells were treated with PCL-PDS NPs (0.5 mg/mL, 200 L per well). After 6 h, 24 h, and 48 h, cells were fixed with buffered formaldehyde (4%), and images were recorded with a Zeiss Axio Cam MRm (Zeiss AG, Oberkochen, Germany) fluorescence microscope.

### 2.9. In vitro cytotoxicity evaluation on MDA-MB-231 cells

A preliminary evaluation of the cytotoxicity profile of CPT-11 was carried out on either MDA-MB-231 breast cancer cells or MCF-10A normal breast epithelium cells. Cells were seeded in 96-well plates at a density of $7.5 \times 10^3$ cells per well and cultured for 24 h in complete DMEM or supplemented DMEM/F-12, respectively. Then the culture medium was replaced with aqueous dispersions of CPT-11 (18 – 1.1 mg $mL^{-1}$), or NPs $DS_{11}CL_{89}$ and NPs $DS_{11}CL_{89}$@CPT-11 at equivalent concentration. After 24 or 48 h of exposure, cell viability was determined using the Cell Titer 96 Aqueous One Solution Cell Proliferation assay (MTS solution, from Promega).

### 2.10. Statistical analysis

The statistical significance of repeated datasets was evaluated using one-way ANOVA, followed by Tukey's post hoc test for single-pair comparisons, performed using GraphPad Prism software. Data were reported as mean value ± S.D., n = 6. Comparisons were considered statistically significant at $p < 0.05$ (*), $p < 0.01$ (**), and $p < 0.001$ (***).

## 3. Results and discussion

### 3.1. Thermal and structural analysis

A comprehensive analysis of the thermal and structural characterization of the copolymers and their corresponding homopolymer was performed to correlate these properties with their performance as drug delivery systems. To cover the entire composition range, three representative samples were synthesized: a PDS-rich copolymer, a PCL-rich copolymer, and one of intermediate composition.

Fig. 1a illustrates the variation of the melting temperature ($T_m$) obtained from the first heating scan after film formation as a function of caprolactone content. A linear decrease in $T_m$ is observed on both sides of the pseudoeutectic point (indicated by the dashed vertical line), confirming the typical V-shaped trend of isodimorphic systems due to the inclusion/exclusion process of one of the comonomers in the dominant crystalline structure. This process also influences the degree of crystallinity ($X_c$), as shown in Fig. 1a (right-hand axis, blue symbols), where a minimum $X_c$ value of approximately 5% is observed at the pseudoeutectic composition ($DS_{11}CL_{89}$). Moreover, the glass transition temperature ($T_g$) was measured (Fig. S2), observing a single value for all the copolymers, as expected for random copolymers.

To confirm the existence of distinct crystalline structures on both sides of the pseudoeutectic region, WAXS analyses were performed. Fig. 1b displays the WAXS patterns obtained at −40 °C after cooling at 20 °C/min. From these data, *d*-spacing (Fig. 1c) was calculated. As shown in Fig. 1b, the *d*-spacing varies systematically with composition on both sides of the pseudoeutectic region, confirming the inclusion of comonomer units into the dominant crystalline phase. Therefore, it is observed that, for $DS_{71}CL_{29}$ and $DS_{44}CL_{56}$ compositions, the samples crystallize with a PDS crystalline unit cell, with some PCL comonomer inclusion, whereas for $DS_{11}CL_{89}$, the crystalline phase corresponds to PCL, with PDS comonomer inclusion. Fig. 1 demonstrates that these copolymers exhibit the typical isodimorphic behavior reported for different random copolyesters [10–15,19,20,26].

The detected differences in thermal behavior (Fig. 1a), crystal structure (Fig. 1b and 1c), and overall crystallinity (Fig. 1a) are expected to significantly influence drug incorporation within the polymer matrix and the stability of the resulting nanoparticles.

### 3.2. Preparation of nanoparticles using DS-CL copolymers

In this work, the sample composition was chosen to span polymeric materials with varying crystalline structures, morphologies, and crystallinities, as explained in the previous section. In this way, it was possible to study how the different nature of the copolymeric samples used affects their drug-delivery properties. Nanoparticles based on the DS-CL copolymers were successfully produced through

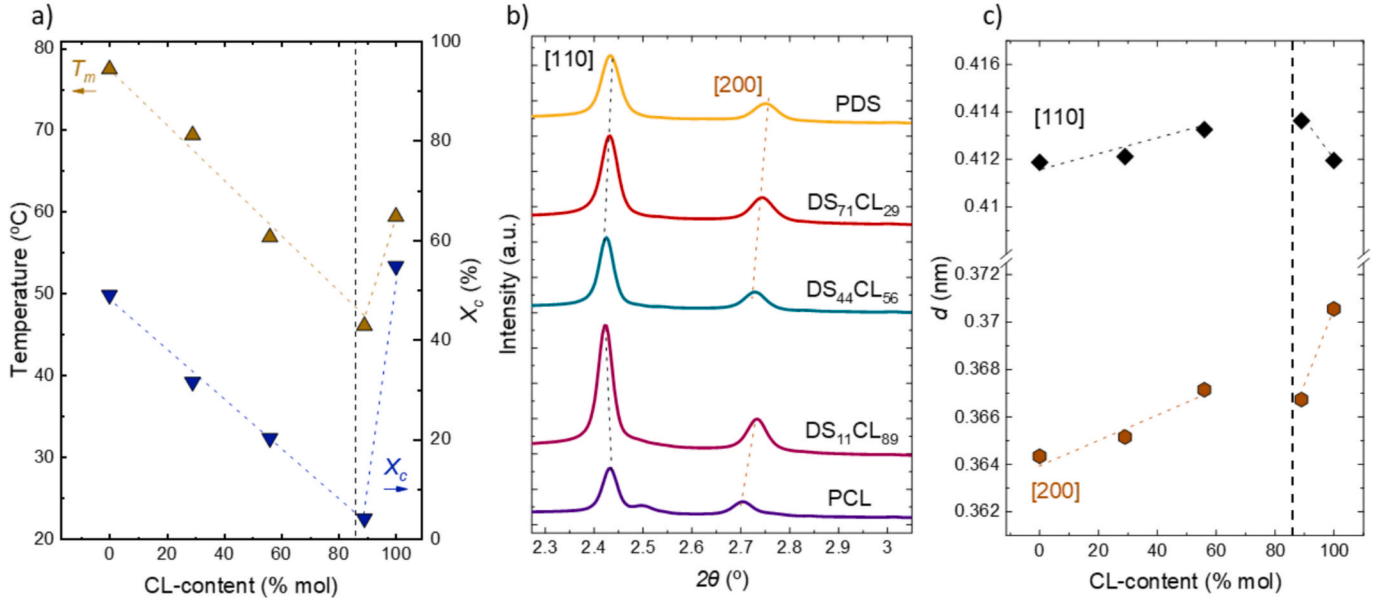


**Fig. 1. Characterization of DS-CL copolymers.** Melting temperature ($T_m$) and degree of crystallinity ($X_c$) against CL-unit content in the copolymers and parent homopolymers (a). The dashed vertical lines indicate the pseudoeutectic point. WAXS diffractograms obtained at −40 °C after a cooling from the melt at 20 °C/min (b). d-spacing variation against CL-content obtained from WAXS measurements (c).

nanoprecipitation, resulting in colloidally stable aqueous dispersions without visible aggregation. Copolymers were dispersed in acetone and treated with an all-at-once addition of water to induce spontaneous nanoparticle formation via solvent displacement. To promote a more sustainable production process and facilitate future industrial optimization, acetone was chosen as a green solvent, since it offers a lower environmental impact than other organic solvents commonly used to dissolve hydrophobic polyesters [27]. After several attempts (Table S1), the nanoprecipitation process parameters were fine-tuned to yield nanoparticles with a mean diameter below 150 nm, enabling efficient drug delivery through the enhanced permeability and retention (EPR) effect. [28] As illustrated in Fig. 2, the STEM micrographs of the DS-CL NPs revealed uniformly spherical nanostructures with the expected size distribution, exhibiting homogeneous morphology and composition, and no evidence of phase segregation.

All three copolymers ($DS_{44}CL_{56}$, $DS_{71}CL_{29}$, and $DS_{11}CL_{89}$) yielded well-dispersed nanoparticles, although some differences in their colloidal behavior were observed, depending on the copolymer composition. Dynamic light scattering (DLS) analysis was performed to assess hydrodynamic size, polydispersity index (PDI), and surface charge (Z-potential) of the resulting formulations (Table 2). Notably, $DS_{71}CL_{29}$ and $DS_{11}CL_{89}$ nanoparticles exhibited the smallest size and a narrow size distribution, indicating excellent colloidal uniformity. In contrast, NPs $DS_{44}CL_{56}$ displayed the largest mean size (142 nm), still maintaining a low PDI (0.008).

Z-potential values were negative for all three formulations, with appropriate absolute values to ensure the stability of the colloidal dispersions due to electrostatic repulsion [29]. Effectively, the evaluation of stability over time performed by monitoring the Z-average of the formulations after 0, 3, 6, and 10 days, showed negligible variations through the observation period and no signs of aggregation (Fig. S3). These findings indicate that the nanoparticles retained their colloidal stability in aqueous suspension for at least 10 days, highlighting their suitability for potential biomedical applications requiring short- to mid-term storage in dispersion.

Presenting average dimensions below 150 nm and ideal Z-potential to ensure long-lasting stability, DS-CL nanoparticles hold promising features as potential nano-dean ideal Z-potential to ensure long-lasting stability, DS-CL nanoparticles exhibit promising features as potential nano-delivery systems [30]. For long-term storage, it is preferable to obtain the nanoparticles in a solid form, allowing the colloidal dispersion to be re-prepared at the time of use [31]. Therefore, the nanoparticle dispersions (1.0 mg $mL^{-1}$) were freeze-dried and then resuspended in ultrapure water. Unfortunately, significant nanoparticle aggregation was observed after freeze-drying, indicating that the process leads to a loss of colloidal stability. To address this issue, we investigated the use of cryoprotectant agents (PEG 4 kDa, 5% w/v, and PEG 10 kDa, 5% w/v) to determine whether they could improve the stability of the formulations, enabling redispersion only when needed and better preserving the structural integrity of the nanoparticles [32] (Table 3).

Among the tested conditions, PEG 4 kDa proved to be more effective in preserving nanoparticle integrity upon rehydration. For instance, nanoparticles with PEG 4 kDa exhibited a moderate increase in size and a slightly higher PDI compared to their pre-lyophilization values, yet remaining within the acceptable range for colloidal stability and drug delivery application. In contrast, PEG 10 kDa was less effective overall: redispersed samples exhibited larger particle sizes and failed in the case of NPs $DS_{11}CL_{89}$ and NPs $DS_{71}CL_{29}$, which showed complete aggregation. These findings highlight the superior performance of PEG 4 kDa as a cryoprotectant for DS-CL-based nanoparticles, likely due to its lower molecular weight, which enables more effective steric stabilization during freezing and drying.

**Table 2**
**Mean size, PDI values, and Z-potential of DS-CL nanoparticles**. Data are reported as mean value ± SD.

| Name | Z-average (nm) ± SD[a] | PDI ± SD[a] | Z-potential (mV) ± SD[a] |
|---|---|---|---|
| NPs $DS_{71}CL_{29}$ | 93 ± 6 | 0.015 ± 0.011 | − 28 ± 10 |
| NPs $DS_{44}CL_{56}$ | 142 ± 1 | 0.008 ± 0.006 | − 28 ± 10 |
| NPs $DS_{11}CL_{89}$ | 100 ± 5 | 0.019 ± 0.010 | − 26 ± 9 |

[a] Obtained by DLS analysis.

**Table 3**
**Characteristic of PCL-PDS nanoparticles in aqueous dispersion after freeze-drying in the presence of cryoprotectants.** Mean size, PDI values, and Z-potential of PCL-PDS nanoparticles with different cryoprotectants after freeze-drying.

| Name | Z-average (nm) | PDI | Z-potential (mV) |
|---|---|---|---|
| NPs $DS_{71}CL_{29}$ + PEG 4 kDa | 127 | 0.093 | −19 ± 5 |
| NPs $DS_{71}CL_{29}$ + PEG 10 kDa | Aggregated | Aggregated | Aggregated |
| NPs $DS_{44}CL_{56}$ + PEG 4 kDa | 197 | 0.172 | − 25 ± 4 |
| NPs $DS_{44}CL_{56}$ + PEG 10 kDa | 301 | 0.124 | −30 ± 4 |
| NPs $DS_{11}CL_{89}$ + PEG 4 kDa | 158 | 0.111 | −15 ± 5 |
| \NPs $DS_{11}CL_{89}$ + PEG 10 kDa | Aggregated | Aggregated | Aggregated |

### 3.3. Incorporation of CPT-11 within DS-CL nanoparticles

Irinotecan (CPT-11) was selected as a model drug to assess the drug-delivery potential of DS-CL nanoparticles for precision medicine in breast cancer. Belonging to the camptothecin class, CPT-11 has been successfully employed in the treatment of various solid tumors, including colorectal, pancreatic lung, ovarian and breast cancer [33]. Despite its efficacy, CPT-11 is characterized by low stability, rapid removal from the body, and dose-dependent side effects. Therefore, nanodrug delivery systems can be employed to enhance drug bioavailability, facilitate controlled and sustained release, and induce passive tumor targeting via the EPR effect, thereby improving therapeutic efficacy while minimizing systemic side effects [34–36].

CPT-11 was loaded into DS-CL NPs during their formation by nanoprecipitation. To strengthen the physical drug-copolymer interactions, the drug and copolymer were mechanically mixed in the organic phase, and nanoprecipitation was then performed in the presence of the drug. During the initial mixing and solvent evaporation steps, the formation of a viscous paste suggested preliminary interactions between the drug and the polymer, facilitating the encapsulation of CPT-11 within the polymer matrix. This procedure was

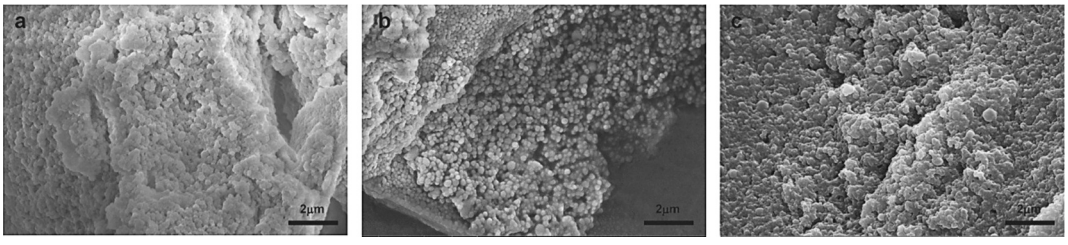


**Fig. 2. STEM micrographs of DS-CL NPs.** STEM micrographs of $DS_{71}CL_{29}$ (a), $DS_{44}CL_{56}$ (b), and $DS_{11}CL_{89}$ (c). Scalebar: 2 m.

successful only with the $DS_{11}CL_{89}$ copolymer, yielding stable nanoparticle dispersions indicated as NPs $DS_{11}CL_{89}$@CPT-11. In contrast, attempts using other copolymers failed due to the loss of nanoparticles' stability immediately after nanoprecipitation. This study supports a clear structure–property–function relationship in isodimorphic DS–CL copolymers and demonstrates how semi-crystalline architecture influences nanoparticle formation and drug affinity. Thermal and structural analyses confirmed the pseudoeutectic behavior, characterized by composition-dependent comonomeric inclusion/exclusion phenomena within the dominant crystalline phases. The degree of crystallinity was not directly measured in the nanoparticles. Therefore, the proposed correlation between copolymer crystalline microstructure and nanoparticle performance should be interpreted primarily in terms of the intrinsic properties of the parent polymers. The crystallinity of isodimorphic copolymers is primarily determined by the balance between comonomer inclusion and exclusion. Thus, we do not expect a significant change in crystallinity between the films and the nanoparticles, although this aspect should be checked in future dedicated studies.

The results described above evidence a higher affinity of the $DS_{11}CL_{89}$ copolymer for CPT-11, underscoring that different copolymer compositions confer diverse drug-complexing abilities. This enhanced affinity may be attributed to the different crystalline structure of the $DS_{11}CL_{89}$ copolymer compared with the other compositions, as discussed in Section 3.1. This is the copolymer with the lowest DS, the more hydrophobic comonomer due to its higher number of methylene groups in its repeating units. It should be recalled that in this copolymer, only PCL-type crystals are formed. The PCL-type crystalline phase appears to promote better interactions with the drug than the PDS-type crystalline phase, which could explain why nanoparticle stability is observed exclusively for this composition. Furthermore, the lower degree of crystallinity in $DS_{11}CL_{89}$ probably facilitates the interaction between the copolymer matrix and CPT-11, resulting in more efficient drug encapsulation and enhanced nanoparticle stability.

HPLC analysis revealed that the loading process was successful, leading to a 7.6 ± 1.2% drug loading (DL %) with a satisfactory encapsulation efficiency (47.0 ± 5.6%). The loading process had a significant impact on the size of the nanoparticles, causing a significant increase in the hydrodynamic diameter (Z-average = 309 ± 20 nm, PDI 0.132 ± 0.012), likely due to the reorganization of the polymeric structure and the formation of physical interactions between CPT-11 and the $DS_{11}CL_{89}$ copolymer. Actually, using a dialysis membrane to remove excess free drug and solvent may have led to structural rearrangement of the nanoparticles, further enhancing their hydrodynamic diameter. The $DS_{11}CL_{89}$@CPT-11 nanoparticles displayed a much more negative zeta potential (− 48.6 mV) compared to the unloaded ones; this shift can be attributed to the presence of ionizable groups of irinotecan hydrochloride at the nanoparticle surface. The physical state of CPT-11 within the nanoparticles was not directly investigated. However, the absence of detectable drug precipitation and the sustained-release profile suggest that the drug is likely dispersed within the polymer matrix in a non-crystalline or molecularly associated form. Further solid-state characterization of the loaded nanoparticles would be required to conclusively determine the physical state of the encapsulated drug.

The drug-release profile of CPT-11 was evaluated to assess the stability of its interaction with the polymeric nanostructure. The analysis was performed in two different pH conditions (5.5 and 7.4), simulating the acidic tumor microenvironment and physiological conditions, respectively. As shown in Fig. 2, $DS_{11}CL_{89}$@CPT-11 nanoparticles exhibited a prolonged, sustained release profile under all tested conditions, reaching approximately 50% drug release after 24 h.

Although the total amount of drug released was comparable, the release kinetics differed notably, indicating pH-dependent release mechanisms. In particular, under buffered saline conditions at pH 7.4, an initial loss of interaction leads to rapid drug release, which reaches a plateau after 6 h. The release kinetics at pH 5.5, instead, show an increasing trend, with no initial burst effect, indicating prolonged drug payload release. The different release kinetics observed between pH 7.4 and pH 5.5 can be explained by considering the pH-dependent physicochemical properties of CPT-11 and its interaction with the hydrophobic polymeric matrix. CPT-11 is known to undergo a reversible pH-dependent equilibrium between its hydrophobic lactone form, which is favored under acidic conditions, and its more hydrophilic carboxylate form, predominant (about 87%) at pH 7.4 [37]. At pH 7.4, the increased fraction of the hydrophilic carboxylate form reduces the affinity of CPT-11 for the polyester matrix, promoting faster diffusion into the surrounding medium and resulting in the observed initial burst release. In contrast, at pH 5.5, the prevalence of the lactone form enhances hydrophobic interactions with the PCL-rich polymeric matrix, leading to stronger drug–polymer association and consequently slower diffusion, which manifests as a more sustained release profile. This hypothesis is in agreement with the more negative Zeta-potential value observed for drug-loaded nanoparticles, which suggests that a fraction of CPT-11 is associated with the nanoparticle surface, thus contributing to the initial release phase. The overall release kinetics appear to be governed primarily by drug partitioning within the polymer matrix and its pH-dependent solubility, rather than by bulk matrix erosion within the investigated timeframe. Therefore, the sustained release behavior at acidic pH is likely the result of a combined effect of enhanced drug–polymer interactions and reduced drug solubility, rather than accelerated polymer degradation. The sustained release under acidic pH is particularly interesting for targeted delivery, as a sustained release at pH 5.5 enhances drug availability in the acidic tumor microenvironment while limiting systemic exposure and associated toxicity.

### 3.4. Biological characterizations

#### 3.4.1. Evaluation of the cytotoxic effect of $DS_{11}CL_{89}$@CPT-11 on normal breast cells and triple negative breast cancer cells

The *in vitro* cytotoxic effect of the NPs $DS_{11}CL_{89}$@CPT-11 was evaluated by using the cell viability assay on normal breast epithelium (MCF-10A) and triple negative breast cancer (MDA-MB-231) cell lines after 24, 48, and 72 h of incubation (Fig. 4). Empty $DS_{11}CL_{89}$ nanoparticles exhibited complete cytocompatibility in MCF-10A at the highest concentration and longest exposure times tested. Cell viability remained at roughly 100% up to 48 h of incubation (Fig. 4a-b) and stayed above the cytocompatibility threshold after 72 h of incubation (≥70%, according to ISO 10993–5) (Fig. 4c). A different trend was observed in the MDA-MB-231 cell line, where empty nanoparticles remained cytocompatible up to 48 h of exposure (Fig. 4d-e), but were barely above the cytocompatibility threshold after 72 h of incubation (68%) (Fig. 4f). This suggests a possible weak cytotoxic effect on TNBC cells under chronic exposure, which may be attributed to cumulative intracellular nanoparticle accumulation and mild *endo*-lysosomal/mitochondrial stress, along with the gradual release of acidic degradation products[38]. On the contrary, the drug-loaded nanoparticles NPs $DS_{11}CL_{89}$@CPT-11 showed a dose-dependent cytotoxic effect after 72 h of incubation, leading to a cell viability of 38.0 ± 6.3% at the higher concentration tested and half-maximal effective concentration ($EC_{50}$) of 14.7 g mL, corresponding to a 0.16 mg $mL^{-1}$ $DS_{11}CL_{89}$@CPT-11 dispersion (Fig. 4f). Compared with the free drug, DS11CL89@CPT-11 nanoparticles exhibited reduced cytotoxicity at all evaluated time points in both cell lines. This effect can be attributed to drug encapsulation and sustained drug release profile in NPs $DS_{11}CL_{89}$@CPT-11 (Fig. 3), which likely results in lower intracellular levels of freely available CPT-11 when cells are exposed to equivalent drug doses.

This behavior highlights the enhanced tolerability of the NPs-based system relative to standard chemotherapeutic treatment and aligns with the typical *in vitro* performance observed for drug delivery systems designed to provide controlled release[40,41].

#### 3.4.2. Cell uptake study on triple negative breast cancer cells

To demonstrate that NPs $DS_{11}CL_{89}$ can exert their effects by releasing

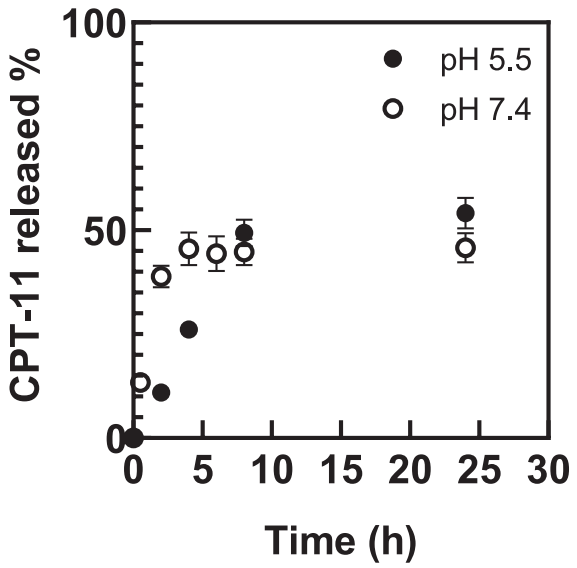


**Fig. 3. Cumulative drug release curves.** Cumulative drug release of CPT-11 from $DS_{11}CL_{89}$@CPT-11 in acidic (pH 5.5, black dots) and physiological (pH 7.4, white dots). Data are reported as mean value ± S.D., n=3.

their payload directly inside cancer cells, cell internalization studies were performed. The internalization of NPs $DS_{11}CL_{89}$ in the MDA-MB-231 breast cancer cell line was assessed using widefield fluorescence microscopy, exploiting the self-trackability of the prepared NPs in DAPI due to its inherent fluorescence (Fig. S4). As shown in Fig. 5, after 24 h of incubation, a diffuse intracellular fluorescence signal was observed, with homogeneous distribution inside cells. In contrast, after 48 h, the signal became more confined and less diffuse, which may be attributed to partial nanoparticle degradation or to exocytosis mechanisms.

These results demonstrate that NPs DS-CL are efficiently internalized by MDA-MB-231 cells within the first 24 h, with potential benefits in terms of intracellular drug release mechanisms. This issue is a matter of great interest for CPT11, since it is a topoisomerase I inhibitor, an important enzyme responsible for relaxing DNA supercoiling during replication and transcription in the S phase[42], which can act only inside the cells.

## 4. Conclusions

This study establishes a clear structure–property–function relationship in isodimorphic DS–CL copolymers and demonstrates how their semicrystalline nature governs nanoparticle formation, drug affinity, and biological performance. Thermal and structural analyses confirmed a pseudoeutectic behavior characterized by composition-dependent inclusion/exclusion phenomena within dominant crystalline phases. The minimum crystallinity observed near the pseudoeutectic composition highlights the tunable structural disorder achievable in this system, providing a powerful handle to modulate drug–polymer interactions. WAXS and DSC results further revealed that subtle variations in comonomer content induce significant changes in thermal properties, unit cell parameters, and degree of crystallinity, ultimately dictating matrix organization at the nanoscale.

All copolymer compositions yielded colloidally stable nanoparticles via a sustainable nanoprecipitation approach using acetone as a low-impact solvent, producing spherical nanostructures of ~ 150 nm in diameter with narrow size distributions. However, composition critically influenced post-processing stability and drug incorporation

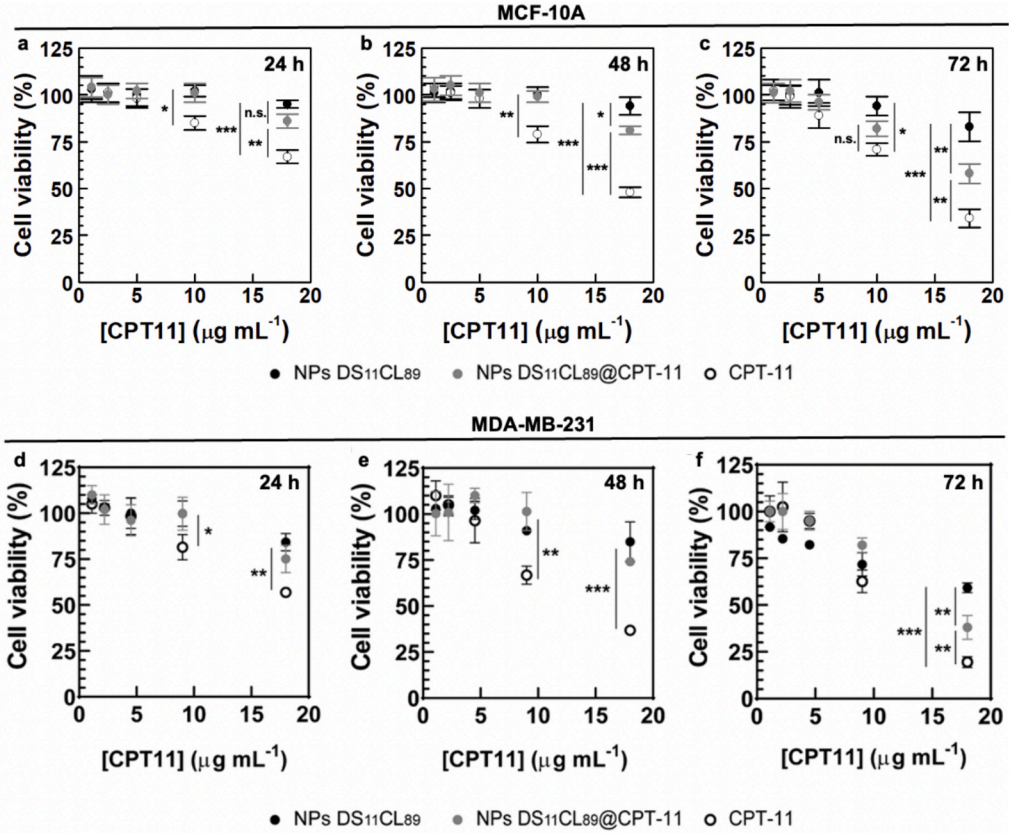


**Fig. 4. Cytotoxic effect of CPT-11 loaded nanoparticles on breast cancer cells.** Results of the cell viability assay performed on MCF-10A (a-c) and MDA-MB-231 (d-f) cells after 24 h, 48 h, and 72 h of incubation with either NPs $DS_{11}CL_{89}$ (black), NPs $DS_{11}CL_{89}$@CPT-11 (gray), or CPT-11 (white). Comparisons were considered statistically significant at $p < 0.05$ (*), $p < 0.01$ (**), $p < 0.001$ (***) (mean ± S.D., n = 3).

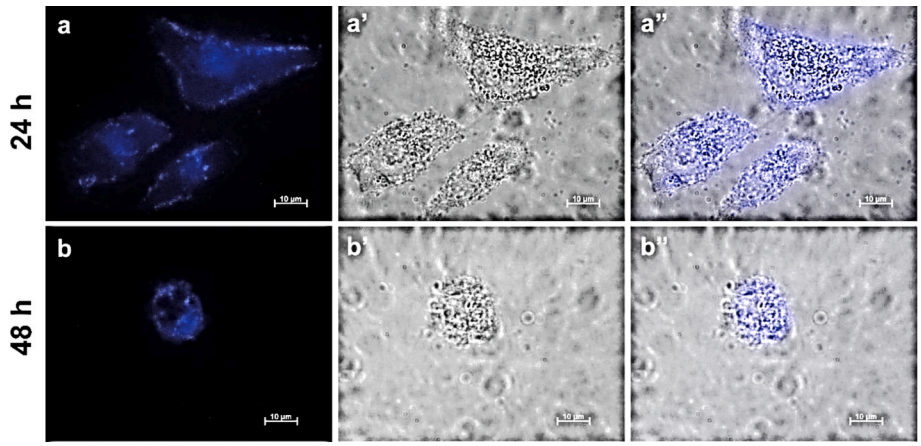


**Fig. 5.** Cellular uptake of NPs $DS_{11}CL_{89}$ on the MDA-MB-231 cell line. Micrographs were acquired after 24 h (a-a') and 48 h (b-b'') of incubation in the DAPI channel, $\lambda_{em} = 377$, $\lambda_{ex} = 477$ (a-b) and compared to brightfield (a'-b') and merge (a''-b'') micrographs. Scalebar: 10 m. 100x magnification.

capability. The PCL-rich $DS_{11}CL_{89}$ copolymer uniquely enabled stable encapsulation of CPT-11, highlighting the decisive role of the crystalline phase and the degree of crystallinity in promoting effective drug–matrix interactions. CPT-11-loaded $DS_{11}CL_{89}$ nanoparticles exhibited satisfactory drug loading and encapsulation efficiency, alongside a sustained release profile. The enhanced negative surface charge after drug loading further suggests the presence of surface-associated ionizable groups contributing to colloidal stability.

Unloaded nanoparticles demonstrated excellent cytocompatibility in normal breast epithelial cells and minimal toxicity in triple-negative breast cancer (TNBC) cells, confirming the intrinsic safety of the polymeric carrier. In contrast, CPT-11-loaded nanoparticles induced a dose-dependent cytotoxic effect in TNBC cells while exhibiting reduced acute toxicity compared to the free drug, consistent with controlled intracellular drug release. Efficient cellular internalization within 24 h further validates the suitability of this platform for delivering intracellularly active therapeutics such as topoisomerase I inhibitors.

Overall, this work highlights the critical importance of crystalline microstructure engineering in biodegradable polyester copolymers for advanced drug delivery applications. By demonstrating that compositional tuning of the repeating unit translates into profound differences in nanoparticle stability, drug encapsulation, and therapeutic performance, this study provides a rational framework for the design of structure-optimized polymeric nanocarriers. The DS–CL platform, particularly at compositions near reduced crystallinity yet retaining structural coherence, emerges as a promising candidate for precision nanomedicine strategies targeting aggressive breast cancer subtypes.

## CRediT authorship contribution statement

**Roberta Cillari:** Writing – review & editing, Writing – original draft, Validation, Software, Methodology, Investigation, Formal analysis, Data curation. **Juan Torres-Rodríguez:** Writing – review & editing, Writing – original draft, Software, Methodology, Investigation, Formal analysis, Data curation. **Sergio Scirè:** Writing – review & editing, Validation, Software, Methodology, Investigation, Formal analysis, Data curation. **Ricardo Pérez-Camargo:** Writing – original draft, Validation, Methodology, Formal analysis, Data curation. **Giuseppina Roscigno:** Writing – review & editing, Writing – original draft, Methodology, Investigation, Formal analysis, Data curation. **Alejandro J. Müller:** Writing – review & editing, Writing – original draft, Supervision, Resources, Methodology, Funding acquisition, Conceptualization. **Nicolò Mauro:** Writing – review & editing, Writing – original draft, Supervision, Resources, Methodology, Investigation, Funding acquisition, Conceptualization.

## Declaration of competing interest

The authors declare that they have no known competing financial interests or personal relationships that could have appeared to influence the work reported in this paper.

## Acknowledgements

R.C. was supported by the Fondazione Umberto Veronesi through the FUV Post-Doctoral Fellowship 2025, under the supervision of N.M.

We thank Dr. Francesca Terracina, Department of "Scienze e Tecnologie Biologiche Chimiche e Farmaceutiche" – University of Palermo, for helping us in performing the DLS study reported in this work.

This UPV/EHU team received funding from: (a) the EFA074/01 - AcroBioPLAST project, which has been 65% co-financed by the European Union through the Interreg VI-A Spain-France-Andorra Programme (POCTEFA 2021-2027), and (b) the project PID2023-149734NB-C22, financed by MCIU/AEI/10.13039/501100011033 and FEDER EU. The authors performed the Synchrotron radiation WAXS experiments at BL11-NCD-SWEET beamline at the ALBA Synchrotron (Proposal Number 2023077645). We also acknowledge the collaboration of the ALBA Synchrotron radiation facilities staff.

## Appendix A. Supplementary data

Supplementary data to this article can be found online at https://doi.org/10.1016/j.eurpolymj.2026.114747. Polycondensation scheme, $^1$H NMR, $T_g$ of copolymers, optimization process for nanoprecipitation, size distribution of nanoparticles over time.

## Data availability

Data will be made available on request.

## References

[1] L.S. Nair, C.T. Laurencin, Biodegradable Polymers as Biomaterials, Prog. Polym. Sci. 32 (8–9) (2007) 762–798, https://doi.org/10.1016/J.PROGPOLYMSCI.2007.05.017.

[2] A.K. Pearce, R.K. O'reilly, Polymers for Biomedical Applications: the Importance of Hydrophobicity in Directing Biological Interactions and Application Efficacy. 22 (2021) 4459–4469, https://doi.org/10.1021/acs.biomac.1c00434.

[3] N. Mauro, M. Andrea Utzeri, A. Sciortino, M. Cannas, F. Messina, G. Cavallaro, G. Giammona, Printable Thermo- and Photo-Stable Poly(D,L-Lactide)/Carbon Nanodots Nanocomposites via Heterophase Melt-Extrusion Transesterification, Chem. Eng. J. 443 (2022) 136525, https://doi.org/10.1016/J.CEJ.2022.136525.

[4] R. Cillari, A. Sciortino, S. Scirè, M. Cannas, F. Messina, N. Mauro, Fluorescence Switching in PH-Responsive Poly(Amidoamine) Hydrogel Networks Containing Gold Nanoparticles and Carbon Nanodots for potential Real-Time Tumor PH

monitoring, ACS Appl. Opt. Mater. (2025), https://doi.org/10.1021/ACSAOM.5C00194.
[5] T.K. Dash, V.B. Konkimalla, Polymeric Modification and its Implication in Drug delivery: Poly-ε-Caprolactone (PCL) as a Model Polymer, Mol. Pharm. 9 (9) (2012) 2365–2379, https://doi.org/10.1021/MP3001952/ASSET/IMAGES/LARGE/MP-2012-001952_0007.JPEG.
[6] R. Cillari, F. Terracina, S. Sciré, N. Mauro, G. Cavallaro, Hybrid Poly (ε-Caprolactone)–Carbon Dot Nanoparticles as Self-Tracking Theranostic Tools for Precise Docetaxel delivery, J. Drug Deliv. Sci. Technol. 117 (34) (2026) 108020, https://doi.org/10.1016/j.jddst.2026.108020.
[7] Z. Li, B.H. Tan, Towards the Development of Polycaprolactone based Amphiphilic Block Copolymers: Molecular Design, Self-Assembly and Biomedical applications, Mater. Sci. Eng. C 45 (2014) 620–634, https://doi.org/10.1016/J.MSEC.2014.06.003.
[8] B. Jeong, Y.H. Bae, D.S. Lee, S.W. Kim, Biodegradable Block Copolymers as Injectable Drug-delivery Systems, Nature 388 (6645) (1997) 860–862, https://doi.org/10.1038/42218;KWRD=SCIENCE.
[9] I. Arandia, N. Zaldua, J. Maiz, R.A. Pérez-Camargo, A. Mugica, M. Zubitur, R. Mincheva, P. Dubois, A.J. Müller, Tailoring the Isothermal Crystallization Kinetics of Isodimorphic Poly (Butylene Succinate-Ran-Butylene Azelate) Random Copolymers by changing Composition, Polymer (guildf). 183 (2019) 121863, https://doi.org/10.1016/j.polymer.2019.121863.
[10] M. Safari, A. Martínez de Ilarduya, A. Mugica, M. Zubitur, S. Muñoz-Guerra, A. J. Müller, Tuning the thermal Properties and Morphology of Isodimorphic Poly [(Butylene Succinate)-Ran-(ε-Caprolactone)] Copolyesters by changing Composition, Molecular Weight, and thermal history, Macromolecules 51 (23) (2018) 9589–9601, https://doi.org/10.1021/acs.macromol.8b01742.
[11] Y. Yu, Z. Wei, L. Zheng, C. Jin, X. Leng, Y. Li, Competition and Miscibility of Isodimorphism and their Effects on Band Spherulites and Mechanical Properties of Poly(Butylene Succinate-Co-Cis-Butene Succinate) Unsaturated Aliphatic Copolyesters, Polymer (guildf). 150 (2018) 52–63, https://doi.org/10.1016/j.polymer.2018.07.024.
[12] H.-M. Ye, J. Wang, C.-S. Wang, H.-F. Li, Unique Isodimorphism of Poly (Decamethylene Succinate-Ran-Decamethylene Fumarate): Large Pseudoeutectic Region and Fantastic Crystallization/Melting Behavior, Macromolecules 52 (4) (2019) 1447–1457, https://doi.org/10.1021/acs.macromol.8b01848.
[13] B. Zhang, Z. Wei, Y. Zhao, R. Che, Y. Wang, X. Leng, Y. Li, Isodimorphic Aliphatic Copolyester as Midblock of Poly(l-Lactide)-based Triblock Copolymers towards Largely Enhanced Impact Toughness, Eur. Polym. J. 111 (2019) 28–37, https://doi.org/10.1016/j.eurpolymj.2018.12.010.
[14] Y. Yu, Z. Wei, Y. Liu, Z. Hua, X. Leng, Y. Li, Effect of Chain Length of Comonomeric Diols on competition and Miscibility of Isodimorphism: a Comparative Study of Poly(Butylene Glutarate-Co-Butylene Azelate) and Poly(Octylene Glutarate-Co-Octylene Azelate), Eur. Polym. J. 105 (2018) 274–285, https://doi.org/10.1016/j.eurpolymj.2018.06.006.
[15] R.A. Pérez-Camargo, I. Arandia, M. Safari, D. Cavallo, N. Lotti, M. Soccio, A. J. Müller, Crystallization of Isodimorphic Aliphatic Random Copolyesters: Pseudo-Eutectic Behavior and Double-Crystalline Materials, Eur. Polym. J. 101 (2018) 233–247, https://doi.org/10.1016/j.eurpolymj.2018.02.037.
[16] Pan, P.; Inoue, Y. Polymorphism and Isomorphism in Biodegradable Polyesters. *Progress in Polymer Science (Oxford)*. July 2009, pp 605–640. https://doi.org/10.1016/j.progpolymsci.2009.01.003.
[17] Zheng, Y.; Pan, P. Crystallization of Biodegradable and Biobased Polyesters: Polymorphism, Cocrystallization, and Structure-Property Relationship. *Progress in Polymer Science*. Elsevier Ltd October 1, 2020. https://doi.org/10.1016/j.progpolymsci.2020.101291.
[18] R.A. Pérez-Camargo, M. Safari, J. Torres Rodríguez, Y. Liao, A.J. Müller, Structure, Morphology and Crystallization of Isodimorphic Random Copolymers: Copolyesters, Copolycarbonates and Copolyamides, Polymer (guildf) 287 (2023), https://doi.org/10.1016/j.polymer.2023.126412.
[19] M. Safari, J. Torres, R.A. Pérez-Camargo, A. Martínez de Ilarduya, A. Mugica, M. Zubitur, H. Sardon, G. Liu, D. Wang, A.J. Müller, How the Aliphatic Glycol Chain Length Determines the Pseudoeutectic Composition in Biodegradable Isodimorphic Poly(Alkylene Succinate-Ran-Caprolactone) Random Copolyesters, Biomacromolecules 25 (11) (2024) 7392–7409, https://doi.org/10.1021/acs.biomac.4c01073.
[20] O.C. Farokhzad, R. Langer, Impact of Nanotechnology on Drug delivery, ACS Nano 3 (1) (2009) 16–20, https://doi.org/10.1021/NN900002M/ASSET/IMAGES/LARGE/NN-2009-00002M_0001.JPEG.
[21] C. Su, Y. Liu, R. Li, W. Wu, J.P. Fawcett, J. Gu, Absorption, distribution, Metabolism and Excretion of the Biomaterials used in Nanocarrier Drug delivery Systems, Adv. Drug Deliv. Rev. 143 (2019) 97–114, https://doi.org/10.1016/J.ADDR.2019.06.008.
[22] X.J. Loh, B.J.H. Yee, F.S. Chia, Sustained delivery of Paclitaxel using Thermogelling Poly(PEG/PPG/PCL Urethane)s for Enhanced Toxicity against Cancer Cells, J. Biomed. Mater. Res. A 100 A (10) (2012) 2686–2694, https://doi.org/10.1002/JBM.A.34198; WGROUP:STRING:PUBLICATION.
[23] Mauro, N.; Utzeri, M. A.; Drago, S. E.; Buscarino, G.; Cavallaro, G.; Giammona, G. Carbon Nanodots as Functional Excipient to Develop Highly Stable and Smart PLGA Nanoparticles Useful in Cancer Theranostics. *Pharmaceutics 2020, Vol. 12, Page 1012* **2020**, *12* (11), 1012. https://doi.org/10.3390/PHARMACEUTICS12111012.
[24] C.G. Pitt, F.I. Chasalow, Y.M. Hibionada, D.M. Klimas, S.A. Aliphatic, I. Polyesters, The Degradation of Poly(ε-Caprolactone) in Vivo, J. Appl. Polym. Sci. 26 (11) (1981) 3779–3787, https://doi.org/10.1002/app.1981.070261124.
[25] R.A. Pérez-Camargo, I. Arandia, M. Safari, D. Cavallo, N. Lotti, M. Soccio, A. J. Müller, Crystallization of Isodimorphic Aliphatic Random Copolyesters: Pseudo-Eutectic Behavior and Double-Crystalline Materials, Eur. Polym. J. 101 (January) (2018) 233–247, https://doi.org/10.1016/j.eurpolymj.2018.02.037.
[26] N.J. Simi, S. Bharathi Bernadsha, Green Chemistry Approaches for Sustainable Synthesis of Polymeric Nanomaterials, Nanotechnology in Plant Sciences 2 (2025) 311–337, https://doi.org/10.1007/978-3-031-84643-4_11.
[27] H. Kang, S. Rho, W.R. Stiles, S. Hu, Y. Baek, D.W. Hwang, S. Kashiwagi, M.S. Kim, H.S. Choi, Size-Dependent EPR effect of Polymeric Nanoparticles on Tumor Targeting, Adv. Healthc. Mater. 9 (1) (2020) e1901223, https://doi.org/10.1002/ADHM.201901223.
[28] D.J. Pochapski, C. Carvalho Dos Santos, G.W. Leite, S.H. Pulcinelli, C.V. Santilli, Zeta potential and Colloidal Stability predictions for Inorganic Nanoparticle Dispersions: Effects of Experimental Conditions and Electrokinetic Models on the Interpretation of results, Langmuir 37 (45) (2021) 13379–13389, https://doi.org/10.1021/ACS.LANGMUIR.1C02056.
[29] Mitchell, M. J.; Billingsley, M. M.; Haley, R. M.; Wechsler, M. E.; Peppas, N. A.; Langer, R. Engineering Precision Nanoparticles for Drug Delivery. *Nature Reviews Drug Discovery 2020 20:2* **2020**, *20* (2), 101–124. https://doi.org/10.1038/s41573-020-0090-8.
[30] W. Abdelwahed, G. Degobert, S. Stainmesse, H. Fessi, Freeze-Drying of Nanoparticles: Formulation, Process and Storage Considerations, Adv. Drug Deliv. Rev. 58 (15) (2006) 1688–1713, https://doi.org/10.1016/J.ADDR.2006.09.017.
[31] A. Umerska, K.J. Paluch, M.J. Santos-Martinez, O.I. Corrigan, C. Medina, L. Tajber, Freeze Drying of Polyelectrolyte complex Nanoparticles: effect of Nanoparticle Composition and Cryoprotectant selection, Int. J. Pharm. 552 (1–2) (2018) 27–38, https://doi.org/10.1016/J.IJPHARM.2018.09.035.
[32] Kciuk, M.; Marciniak, B.; Kontek, R. Irinotecan—Still an Important Player in Cancer Chemotherapy: A Comprehensive Overview. *International Journal of Molecular Sciences 2020, Vol. 21, Page 4919* **2020**, *21* (14), 4919. https://doi.org/10.3390/IJMS21144919.
[33] C. Scialabba, A. Sciortino, F. Messina, G. Buscarino, M. Cannas, G. Roscigno, G. Condorelli, G. Cavallaro, G. Giammona, N. Mauro, Highly Homogeneous Biotinylated Carbon Nanodots: Red-Emitting Nanoheaters as Theranostic Agents toward Precision Cancer Medicine, ACS Appl. Mater. Interfaces 11 (22) (2019) 19854–19866, https://doi.org/10.1021/acsami.9b04925.
[34] S. Fathi-Karkan, M. Qindeel, R. Arshad, Z. Moafian, E. Ghazy, A. Rahdar, S. Ghotekar, Recent Advancements in Irinotecan-Loaded Nanomaterials as a Smart Drug delivery System for Cancer Therapy: a State-of-Art-Review, Inorg. Chem. Commun. 161 (2024) 112028, https://doi.org/10.1016/J.INOCHE.2024.112028.
[35] A. Wang-Gillam, R.A. Hubner, J.T. Siveke, D.D. Von Hoff, B. Belanger, F.A. de Jong, B. Mirakhur, L.T. Chen, NAPOLI-1 phase 3 Study of Liposomal Irinotecan in Metastatic Pancreatic Cancer: final overall Survival Analysis and Characteristics of Long-Term Survivors, Eur. J. Cancer 108 (2019) 78–87, https://doi.org/10.1016/j.ejca.2018.12.007.
[36] Deng, B.; Kong, Y.; Ma, Y.; Zhan, Y.; Sun, Y.; Wang, R.; Huang, P.; Liu, L. A Novel Carrier-Free Nanoparticle with Stable Distinctive Three-Dimensional Structure for Tumor-Targeted Precision Chemoimmunotherapy. *Journal of Nanobiotechnology 2025 23:1* **2025**, *23* (1), 480-. https://doi.org/10.1186/s12951-025-03568-8.
[37] S. Palakurthi, Challenges in SN38 Drug delivery: Current Success and Future Directions, Expert Opin. Drug Deliv. 12 (12) (2015) 1911–1921, https://doi.org/10.1517/17425247.2015.1070142.
[38] M. Lozano-García, E. Dikici, D. Bilbao, P. Mohan, S. Deo, S. Daunert, Multifunctional delivery strategies and Nanoplatforms of SN-38 in Cancer Therapeutics, J. Control. Release 384 (5) (2025) 113937, https://doi.org/10.1016/j.jconrel.2025.113937.